Trapping Atoms in a Gravitational Cavity

H. Wallis*, **J. Dalibard, and C. Cohen-Tannoudji**

Laboratoire de Spectroscopie Hertzienne de l'E.N.S.** and Collège de France, 24, rue Lhomond,
F-75231 Paris Cedex 05, France

Abstract. This paper is devoted to the study of a new atomic cavity consisting of a single horizontal concave mirror placed in the earth gravitational field. Gravity, by bending the atomic trajectories, plays the role of a second mirror closing the cavity. We first discuss the stability criterion for this cavity, assuming that the mirror has a parabolic shape. We then derive the quantum mechanical modes of such a configuration, with particular emphasis on the paraxial (i.e., close to vertical) motion. Finally, we discuss the possibility of populating those modes from an initial cold atomic cloud dropped above the mirror.

PACS: 32.80.Pj

Besides the elimination of the Doppler effect, laser cooling of free neutral atoms [1] has enhanced by orders of magnitudes the time available for probing atomic particles. Ultraslow atoms have been used to realize Zacharias' proposal of atomic fountains for Ramsey-type microwave spectroscopy [2, 3]. In addition, the capability of storing atoms for a long time paves the way for achieving high densities in atomic traps. The maximal density of laser cooled atoms is now mainly limited by light assisted atomic collision processes [4].

One interest in studying ultracold gases at high densities is the possibility of observing quantum statistical effects. When the extension of the center-of-mass wave packet equals the mean inter-atomic distance, the indiscernability of the particles strongly modifies their collective behavior. For Bosons, an example of such phenomena is the long sought Bose-Einstein condensation of spin-polarized hydrogen [5, 6].

Besides the Bose-Einstein condensation there exist other possibilities for populating discrete quantum states by an average of more than one particle per state. A very prominent one is the state of a laser cavity pumped above threshold, containing more than one, usually a huge number of photons in one or a few modes. It is therefore very appealing to try to duplicate this scheme for atomic particles, by constructing an atomic cavity which would provide discrete levels, long storage times and the possibility of populating a small number of modes (not necessarily the ground one) by more than one atom per mode.

To build such an atomic cavity, it has been recently proposed [7] to use atomic mirrors formed by an evanescent laser wave [8, 9][1]. This provides a potential step which rises nearly instantaneously, i.e., with a length scale small compared to the cavity length. The cavities considered in [7] are a direct duplication of cavities for light. The atomic velocities are assumed to be large enough so that gravity plays a little role in the atomic dynamics.

In contrast, we study in this paper a single mirror cavity in which gravity plays an essential role: it replaces the second missing mirror by bending the atomic trajectories so that the atoms always bounce on the mirror as if on a trampoline (see Fig. 1). A first experiment on such a reflection of falling atoms has been realized recently [11]. Since a plane mirror was used, the confinement time was mainly limited by the transverse motion out of the reflecting spot. Here, we study the case of a concave parabolic mirror which leads to a stable atomic motion and to well defined three-dimensional modes. The main advantage of a gravitational cavity is that it can operate with atoms that are slower ($v_1 \simeq 30$ cm/s) than for the two-mirror cavity ($v_2 \simeq 2$ m/s). The required laser intensity

---

* Present address: Institut für Angewandte Physik der Universität Bonn, Wegelerstrasse 8, W-5300 Bonn, Fed. Rep. Germany
** Laboratoire associé au CNRS et à l'Université Pierre et Marie Curie

[1] Another type of mirror has been demonstrated recently for hydrogen atoms using a film of liquid helium as a reflecting surface [10]
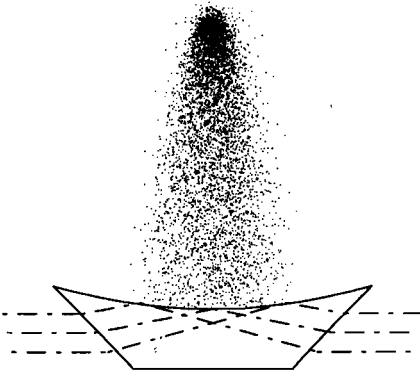
Fig. 1. Principle of trapping atoms in the gravitational field using an atomic mirror. The reflection potential is provided by an evanescent laser wave. Atoms are released above the mirror from an optical molasses or a magnetooptical trap

used for the evanescent waves reflecting the atoms is then much smaller [by a factor $(v_1/v_2)^2$].

For a two-mirror cavity the calculation of the mode structure directly follows from the one done for an optical cavity: one just has to replace the optical wavelength by the atomic de Broglie wavelength which remains nearly constant if the velocity changes due to gravity are small enough. In a one-dimensional gravitational cavity, the direct application of the formalism developped for optical cavities is no longer possible. In this paper we give a quantum mechanical description of the 3D-center-of-mass motion [12], in order to find the eigenfunctions or modes of the cavity, the distribution of its energy levels, and the factor of overlap of the cavity modes with initial atomic wavepackets released from a source of cold atoms. We put special emphasis on this last point since the ultimate goal is to accumulate more than one atom per cavity mode. On the other hand, we shall not discuss here the factors of losses out of the cavity. Indeed these losses, that can be due to momentum diffusion, diffraction losses or collisions, have been studied in detail in [7] and this discussion remains valid for the cavity of interest here.

The paper is organized as follows: In Sect. 1 we recall the solutions for the one-dimensional modes of atoms in an idealized wedge-shaped potential. In Sect. 2 the general three-dimensional problem is treated both classically and quantum mechanically using the separability of this particular problem in parabolic coordinates. The limiting case of the paraxial motion is investigated in detail and *Gaussian modes*, in analogy to optical cavities, are then re-derived. Finally, in Sect. 3 the overlap of the modes with an initial atomic distribution is calculated and the results are discussed. The critical density of atoms confined in the cavity is compared to the critical density of Bose-Einstein condensation.

1 Plane Mirror Modes

We start from a simplified potential corresponding to an instantaneous 100% reflection off a plane atomic mirror and write the Hamilton operator in one dimension as:

$$H = \frac{p^2}{2m} + V(z); \qquad V(z) = \begin{cases} mgz & \text{for } z \geq 0, \\ \infty & \text{for } z < 0. \end{cases} \qquad (1)$$

By setting the potential to infinity at $z = 0$ we idealize the actual reflecting potential step which may be realized by an evanescent light wave whose extension is typically in the μm-range. Such an approximation could be treated in more detail by ascribing a *quantum defect* to the atomic eigenstates that would account for the real short-range repulsive potential and that would vary slowly in the small energy range of interest. We also neglect here the internal evolution due to the interaction with the mirror.

The corresponding stationary Schrödinger-equation is scaled in a convenient way by

$$z_0 = \left(\frac{\hbar^2}{2m^2 g}\right)^{1/3}, \qquad (2)$$

thus reading

$$\psi''(\zeta) - (\zeta - \zeta_E)\psi(\zeta) = 0, \qquad (3)$$

where $\zeta = z/z_0$, $\zeta_E = z_E/z_0$, and $z_E = E/mg$.

The normalizable solutions of this equation are obtained by an appropriate displacement of the Airy-function $Ai(\zeta)$ [13]

$$\psi_n(\zeta) = Ai(\zeta - \zeta_n) \qquad (4)$$

such that the displacement ζ_n of the n-th eigenvector coincides with the n-th zero of the Airy-function $(Ai(-\zeta_n) = 0)$ and ensures the boundary condition $\psi_n(0) = 0$ at the origin. The eigenenergies are correspondingly

$$E_n = mgz_n.$$

The potential and the first eigenfunctions are depicted in Fig. 2.

The dependence of the essential physical features on n becomes more transparent if we turn to the semiclassical quantization of the problem. Using the quasi-classical wavevector

$$k(z) = \sqrt{2m^2 g \hbar^{-2}(z_E - z)} = \sqrt{(z_E - z)/z_0^3} \qquad (5)$$

one obtains as quasi-classical wave-function in the allowed region $z < z_E$:

$$\psi_{WKB}(z) = \frac{1}{\sqrt{k(z)}} \sin\left(\int_z^{z_E} k(z')\,dz' + \pi/4\right). \qquad (6)$$
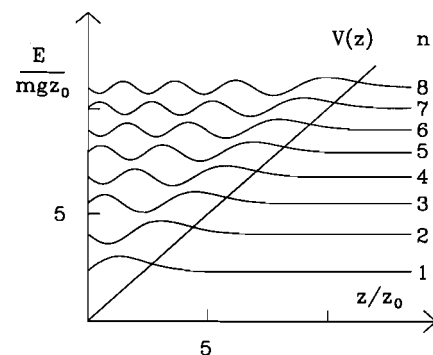
Fig. 2. Eigenfunctions and eigenenergies (quantum number n) of a particle with mass m in a gravitational potential $V(z) = mgz$ with an infinite step at the origin. $z_0 = (\hbar^2/2m^2 g)^{1/3}$ is the quantum length scale

Table 1. Parameters of the gravitational cavity for 3 typical elements for which laser cooling has been achieved. z_0 and ω_0 are the length and frequency scales of the longitudinal quantum motion (2, 12). Considering atoms released at an altitude 5 mm above the mirror, we get an average quantum number $\bar{n}$ for the excitation of the longitudinal motion (Sect. 1). Assuming a radius of curvature $R_M = 2$ cm for the mirror, a cloud of transverse extension $x_i = 1$ mm, and a velocity spread $v_{x_i} = 3v_{rec}$, where v_{rec} is the recoil velocity associated with the cooling transition, we get the classical size of the spot on the mirror ϱ_M (38). $w(z=0)$ is the waist of the ground state mode for the transverse motion with the same longitudinal energy (80)

	He*	Na	Cs
z_0 [µm]	2.33	0.73	0.23
$\omega_0/2\pi$ [Hz]	650	1160	2080
$\bar{n}$	2.1×10^4	1.2×10^5	6.8×10^5
v_{rec} [cm/s]	9.1	3.0	0.35
ϱ_M [cm]	1.2	0.42	0.15
$w(z=0)$ [µm]	32	13	5.6

The WKB quantization condition now reads

$$\int_0^{z_n} k(z')\,dz' = \left(n - \frac{1}{4}\right)\pi, \quad n \geq 1, \tag{7}$$

where z_n is the turning point of the classical motion with energy E_n. Noting that

$$\int_z^{z_E} k(z')\,dz' = \frac{2}{3}\left(\frac{z_E - z}{z_0}\right)^{3/2} \tag{8}$$

we get

$$z_n = z_0 \left[\frac{3\pi}{2}\left(n - \frac{1}{4}\right)\right]^{2/3}. \tag{9}$$

The quantity $(3\pi/2)^{2/3}z_0$ determines the spatial scale of the modes. The distance between neighbouring allowed turning points scales for large n as

$$z_n - z_{n-1} \simeq \pi z_0 \left(\frac{z_0}{z_n}\right)^{1/2} \simeq z_0 \left(\frac{2\pi^2}{3n}\right)^{1/3}. \tag{10}$$

The eigenenergies are given in the WKB-approximation by

$$E_n = \hbar\omega_0 \left(n - \frac{1}{4}\right)^{2/3} \tag{11}$$

with

$$\omega_0 = \left(\frac{9\pi^2 mg^2}{8\hbar}\right)^{1/3}. \tag{12}$$

The splitting between two adjacent energy levels is

$$E_n - E_{n-1} \simeq \frac{\partial E_n}{\partial n} \simeq \frac{2\pi\hbar}{T_{class}}, \tag{13}$$

where $T_{class} = 2(2z_n/g)^{1/2}$ is the period of the classical motion of energy E_n. This splitting decreases as $n^{-1/3}$ for large n. Finally, we indicate in Table 1 the numerical values of those relevant parameters for a few atoms for which laser cooling has been demonstrated and which therefore are good candidates for populating such a trap:

metastable helium in the ^3S state, sodium, and cesium. To estimate the average quantum number, we have assumed in Table 1 that the atoms are dropped from a height $z_E = 5$ mm above the mirror $(1/T_{class} = 15.7$ Hz).

2 Parabolic Mirror Modes

To confine the motion in the cavity, it is necessary to compensate for the transverse escape of the bouncing particles. A concave parabolic mirror, corresponding to a potential V such as

$$V = \infty \quad \text{if} \quad z < \frac{x^2 + y^2}{2R_M}, \tag{14}$$

where R_M is the radius of curvature of the mirror at its center, serves this purpose very well. This parabolic mirror is assumed to be infinite so that the gravitational potential provides a stable trapping of the atoms for any initial condition.

The aim of this section is to give a quantum mechanical description of the problem, i.e., to derive eigenvalues and eigenstates of the Hamiltonian. However, it is instructive to start with a classical analysis of the trajectories. This is done first in a paraxial approximation and second for the general case. Here we use parabolic coordinates for which the equations of motion, including the reflection off the mirror, are separable. We then study the quantum problem also in parabolic coordinates and focus onto paraxial states. Finally, we conclude this section by pointing out the similarities and the differences between our treatment and the Gaussian beam approach for the study of optical cavities in the paraxial regime.

2.1 Simplified Stability Consideration

We are interested here in a configuration where the classical trajectories of a particle bouncing off the mirror are stably confined to a small, paraxial region of the mirror. This paraxial domain is more precisely characterized by a small ratio between horizontal and longitudinal velocity components and by a transverse position spread on the mirror that is small compared to the height of the trajectories. For simplicity we consider here a motion in the x–z-plane, i.e., with no angular momentum along the z-axis.

To study the stability of a multiply reflected trajectory one can use a simple approach analogous to the study of stability of an optical cavity [14]. The time evolution of the transverse atomic coordinate is modeled by the iteration of a 2×2 propagation matrix for the position x_n and the velocity v_{xn} of the particle at the mirror. Assuming that both the modulus v_z of the vertical velocity component on the mirror and the time of flight $2v_z/g$ between two successive bounces remain nearly constant, we obtain the iterated map

$$\begin{pmatrix} x_{n+1} \\ (v_x)_{n+1} \end{pmatrix} = M \begin{pmatrix} x_n \\ v_{xn} \end{pmatrix} \tag{15}$$

with

$$M = \begin{pmatrix} 1 & 2v_z/g \\ -2v_z/R_M & 1-4v_z^2/(R_Mg) \end{pmatrix}. \tag{16}$$

The iteration of the unimodular 2×2 matrix M is stable for the condition $|\text{Tr}(M)| < 2$. This is fulfilled if

$$v_z^2 < R_Mg. \tag{17}$$

Introducing the apex $h = v_z^2/2g$ of the trajectory we can rewrite this as

$$h < \frac{R_M}{2}. \tag{18}$$

Thus, stable paraxial motion is possible if the apex stays *below* the focus F of the mirror.

2.2 The Classical Motion in Parabolic Coordinates

We now turn to the study of the classical motion in the general case, where the horizontal velocity components are comparable in magnitude with the vertical components. The apparent complexity of the classical motion under multiple reflections can be considerably reduced by finding the constants of the motion. Two of them are obvious: the energy E and the z-component of the angular momentum due to the rotational symmetry around the z-axis. Both of them are also conserved after reflection from the mirror.

For a linear potential such as $V = mgz$ there exists, as for the Kepler-problem, a third independent quantity

$$b = \frac{1}{m}\left[\mathbf{p} \times \mathbf{L} + \frac{m^2g}{2}\mathbf{r} \times (\mathbf{r} \times \mathbf{e}_z) \right] \cdot \mathbf{e}_z$$

$$= \frac{1}{m}\left[\tilde{z}(p_x^2 + p_y^2) - (xp_x + yp_y)p_z - m^2g\frac{x^2+y^2}{2} \right] \tag{19}$$

which remains constant during free motion. The existence of this constant of the motion is analogous to the conservation of the Runge-Lentz vector of the Kepler-problem [15]. Note that in (19) we have shifted the origin of the z-axis into the focus F by setting

$$\tilde{z} = z - \frac{R_M}{2} \tag{20}$$

and that we have defined the angular momentum L with respect to F.

The important property of the parabolic mirror which we show in the following is that b is also conserved after reflection off the mirror, and is thus a constant of the entire motion [16]. To take advantage of this symmetry we now turn to the formulation of the problem in parabolic coordinates. This will allow us to separate the 3D problem into three 1D problems, both for the classical and the quantum case.

The *parabolic coordinates* ξ, η, ϕ are defined with respect to the focus as:

$$\tan \phi = x/y,$$

$$\xi = \sqrt{x^2 + y^2 + \tilde{z}^2} + \tilde{z}, \tag{21}$$

$$\eta = \sqrt{x^2 + y^2 + \tilde{z}^2} - \tilde{z}.$$

The surfaces of constant parabolic coordinates ξ and η are paraboloids around the z-axis, having a common focus F and radii of curvature ξ and η on axis:

$$\tilde{z} = \frac{\xi}{2} - \frac{x^2+y^2}{2\xi},$$

$$\tilde{z} = -\frac{\eta}{2} + \frac{x^2+y^2}{2\eta}. \tag{22}$$

In particular, the surface of the mirror is described by $\eta = R_M$.

The parabolic *momenta* are now position dependent and defined by

$$p_\xi = m\dot{\xi}\frac{\xi+\eta}{4\xi} \quad \text{and} \quad p_\eta = m\dot{\eta}\frac{\xi+\eta}{4\eta}. \tag{23}$$

They are related to the cartesian momenta by

$$p_{\xi,\eta} = \frac{1}{2}\left(\frac{xp_x + yp_y}{r \pm \tilde{z}} \pm p_z \right) \quad \text{and} \quad p_\phi = xp_y - yp_x = L_z, \tag{24}$$

where $r = (x^2 + y^2 + \tilde{z}^2)^{\frac{1}{2}}$ and where the $+$ $(-)$ sign stands for ξ (respectively η).

The three constants of motion can be calculated in parabolic coordinates

$$\tilde{E} = \frac{1}{m}\left[2\frac{\xi p_\xi^2 + \eta p_\eta^2}{\xi + \eta} + \frac{p_\phi^2}{2\xi\eta} + \frac{m^2g}{2}(\xi - \eta) \right], \tag{25}$$

$$L_z = p_\phi, \tag{26}$$

and

$$b = \frac{1}{m}\left[2\frac{\xi\eta(p_\eta^2 - p_\xi^2)}{\xi + \eta} + \frac{p_\phi^2(\xi - \eta)}{2\xi\eta} - \frac{m^2g}{2}\xi\eta \right]. \tag{27}$$

The potential energy $U = mg(\xi - \eta)/2$ and the energy $\tilde{E}$ are measured with respect to the focus. For the 1D motion along the z-axis, $\tilde{E}$ is related to the energy E introduced in Sect. 1 by $\tilde{E} = E - mgR_M/2$.

The transformation of the canonical momenta in a reflection on the parabolic mirror is particularly simple in parabolic coordinates

$$p_\xi \to p_\xi, \quad p_\eta \to -p_\eta, \quad p_\phi \to p_\phi. \tag{28}$$

As a consequence of (28) all three constants of the motion are conserved under reflection.

Combining (25) and (27) to form the quantities $\tilde{E} + b/\eta$ and $\tilde{E} - b/\xi$, we now get two independent equations for the momenta p_ξ and p_η:

$$p_\xi^2 = \frac{m}{2}(\tilde{E} - U_1(\xi)), \tag{29}$$

$$p_\eta^2 = \frac{m}{2}(\tilde{E} - U_2(\eta)) \tag{30}$$
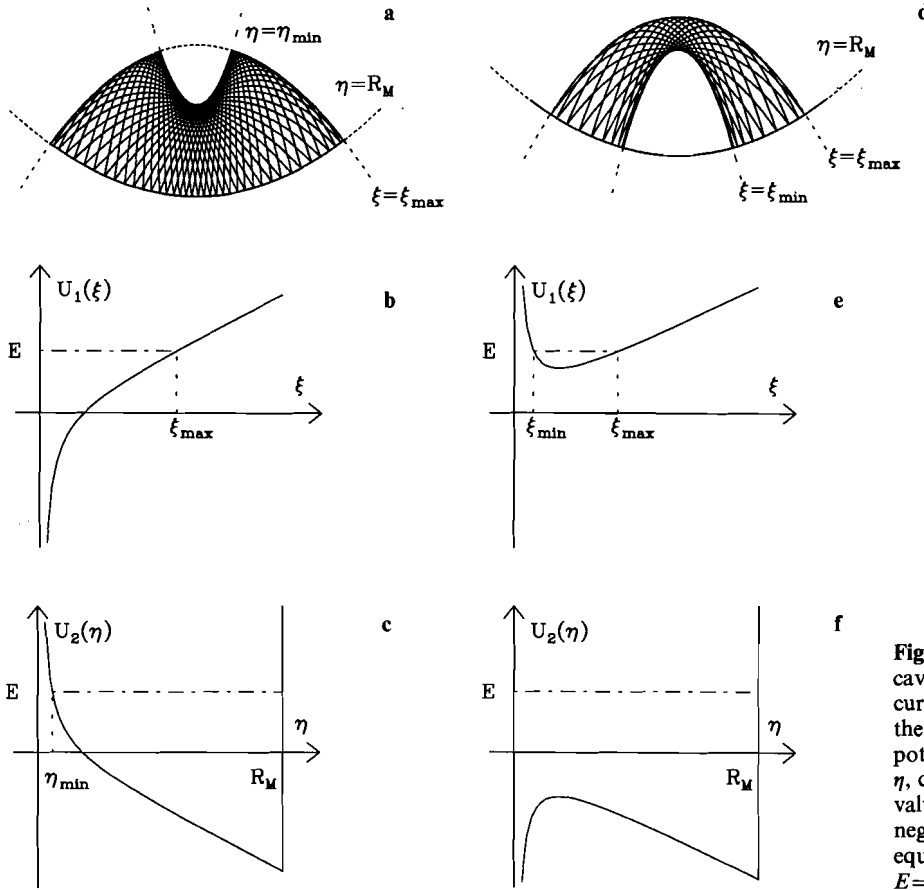
Fig. 3a–f. Classical motion in a gravitational cavity using a parabolic mirror with radius of curvature R_M. a and d: atomic trajectories in the x–z-plane. b, c, and e, f show the effective potentials for the parabolic coordinates ξ and η, corresponding to a and d, respectively. The value of the constant of the motion b is negative for a–c, and positive for d–f, with equal modulus $|b| = 0.164 mg R_M^2$. In both cases $E = 0.25 mg R_M$

with effective potentials U_1 and U_2 that depend on the constants L_z and b:

$$U_1(\xi) = \frac{mg\xi}{2} + \frac{b}{\xi} + \frac{L_z^2}{2m\xi^2}, \tag{31}$$

$$U_2(\eta) = -\frac{mg\eta}{2} - \frac{b}{\eta} + \frac{L_z^2}{2m\eta^2}. \tag{32}$$

In addition to the gravity and centrifugal potentials, one thus obtains apparent "Coulomb terms" b/ξ and b/η.

The separability of the problem in parabolic coordinates plays an essential role for the analysis of the motion. Suppose that we start with atoms on the z-axis $(x = y = 0)$ with $v_z = 0$, at an altitude h above the mirror, and with a velocity v_x along the x-axis. Such a two-dimensional situation corresponds to $L_z = 0$. Then the sign of b, as calculated from (19), is directly related to the position of the launching point with respect to the focus; if the atom starts from below the focus $(\tilde{z} < 0)$, b is negative, if it starts from above $(\tilde{z} > 0)$, b is positive. As a consequence, for negative b the potential $U_1(\xi)$ tends to $-\infty$ for $\xi \to 0$ and the trajectory in ξ-space is confined between $\xi = 0$ (corresponding to the negative $\tilde{z}$-axis) and an outer turning point ξ_{max} (Fig. 3b). As can be seen from Fig. 3c, the η-motion is confined between a parabola η_{min} and $\eta = R_M$. A corresponding trajectory in the x–z-plane is shown in Fig. 3a.

On the other hand, for positive b (and still $L_z = 0$), $U_1(\xi) \to +\infty$ if $\xi \to 0$ so that the equation $\tilde{E} - U_1(\xi) = 0$ has two positive roots $\xi_{min} = \xi_-$ and $\xi_{max} = \xi_+$ given by

$$\xi_\pm = (\tilde{E} \pm \sqrt{\tilde{E}^2 - 2mbg})/mg \tag{33}$$

if $\tilde{E} > \sqrt{2mbg}$; the ξ-motion is then confined between an inner and an outer turning point (Fig. 3e). The η-motion is confined between 0 and R_M (Fig. 3f) and the corresponding x–z-motion is therefore bounded by the three parabolas $\xi = \xi_{min}$, $\xi = \xi_{max}$, and $\eta = R_M$ (Fig. 3d).

Using the above analysis, we can rederive the stability condition (18) as a consequence of the sign of b. If b is negative (particle dropped on the z-axis above the focus), the motion excludes the negative z-axis and is never paraxial. On the other hand, if b is negative with a small absolute value (particle dropped below the focus with a small transverse velocity v_x), the ξ-motion is confined between 0 and $\xi_{max} \ll R_M$, which corresponds to a paraxial motion along the negative z-axis.

The knowledge of the constants of the motion also allows us to determine the area on the mirror that is hit during the multiple reflections occurring for a given classical trajectory. This is an important quantity in practice since it determines the size of the spot over which one has to ensure a good reflectivity. As an example, we consider again an atom dropped at a height $h < R_M/2$ above the mirror with $v_z = 0$. We assume here that both the initial displacement x_i and the initial velocity v_{xi} along the

x-axis are non-zero. The three constants of the motion take the values:

$$\tilde{E} = m\frac{v_{xi}^2}{2} + mgh - \frac{mgR_M}{2}, \tag{34}$$

$$L_z = 0, \tag{35}$$

$$b = -mv_{xi}^2\left(\frac{R_M}{2} - h\right) - \frac{mgx_i^2}{2}, \tag{36}$$

b and $\tilde{E}$ are assumed to be negative so that the motion is of the type sketched in Fig. 3a. From the relation $x^2 + y^2 = \xi\eta$ (with $y = 0$ in our particular example) we can determine the extension ϱ of the transverse motion. Close to the upper turning point the maximal radius, corresponding to the intersection of the two boundary parabolas, is given by $\varrho_S^2 = \xi_{max}\eta_{min}$, and reads (without any approximation) as

$$\varrho_S^2 = -\frac{2b}{mg}$$

$$= x_i^2 + (R_M - 2h)\frac{v_{xi}^2}{g}. \tag{37}$$

Similarly, the spot size on the mirror ($\eta = R_M$) is given by $\varrho_M^2 = \xi_{max}R_M$:

$$\varrho_M^2 = \frac{R_M}{mg}(\sqrt{\tilde{E}^2 - 2mbg} + \tilde{E}) \tag{38}$$

which, in the paraxial limit $v_{xi}^2/2g$, $x_i \ll (R_M/2) - h$, can be simplified into

$$\varrho_M \simeq \sqrt{R_M\left(\frac{v_{xi}^2}{g} + \frac{x_i^2}{R_M - 2h}\right)}. \tag{39}$$

To give a short numerical example we consider the three atoms mentioned above (He*, Na, Cs) each cooled at an rms velocity equal to 3 times the recoil velocity $v_{rec} = \hbar k/m$, which is known to be of the order of the minimal velocity dispersion achievable with optical molasses [17–19]. We take a parabolic mirror with $R_M = 2$ cm ($OF = 1$ cm), and we assume that the initial atomic cloud is dropped from a height $h = 5$ mm above the mirror surface with a spatial extension $x_i = 1$ mm. The values for v_{rec} and ϱ_M are indicated in Table 1. We note that for He* and Na the initial conditions do not fulfill the requirement for a paraxial motion. However, the exact result from (38) is found to be close to the approximate one (39). The leading term in ϱ_M comes from the x_i^2 term for Cs, and from the v_{xi}^2 term for He* and Na.

Note finally, that classically x_i^2 and v_{xi}^2 can both be arbitrarily small, so that there is no lower bound to ϱ_S and ϱ_M, the bouncing motion remaining in this limit even linear along the z-axis. Quantum mechanically, the Heisenberg uncertainty relation $mx_iv_{xi} \geq \hbar/2$ imposes a lower bound for ϱ_S and ϱ_M which is found to be

$$\varrho_S^{min} = [2z_0^3(R_M - 2h)]^{1/4} \tag{40}$$

and

$$\varrho_M^{min} \simeq \sqrt{\frac{R_M}{R_M - 2h}}\varrho_S^{min}. \tag{41}$$

Later on we will confirm these heuristic estimates by a full quantum mechanical treatment, ϱ_S and ϱ_M appearing as the beam waists of the fundamental transverse mode at the turning point and at the mirror (79, 80). ·

2.3 Quantum Mechanics of Atoms Bouncing off a Parabolic Mirror

We now turn to the quantum mechanical description of the motion. We assume that the mirror is infinite and that the motion is bound in three dimensions, so that the entire spectrum is discrete. In practice the mirror will be finite and there will still exist a continuous part of the energy spectrum; also unavoidable losses will limit the lifetime of the trapped particles and will give a width to the levels. However, these effects will be neglected here.

We have seen in the previous section that in the classical regime there are three constants of the motion, $\tilde{E}$, L_z, and b. The corresponding quantum mechanical property is the existence of three operators which commute and can have a common basis set of eigenvectors. The operator corresponding to b is obtained by symmetrizing $\mathbf{p} \times \mathbf{L}$ in the well known manner yielding $(\mathbf{p} \times \mathbf{L} - \mathbf{L} \times \mathbf{p})/2 = \mathbf{p} \times \mathbf{L} - i\hbar\mathbf{p}$. The eigenfunctions of the Hamiltonian can thus be labelled $\Psi_{\tilde{E},M,b}$ corresponding to the eigenvalues $\tilde{E}$, $\hbar M$, and b. Here M is integer (M and $-M$ are degenerate) whereas $\tilde{E}$ and b are real numbers.

When determining the solutions of the stationary Schrödinger equation, we also take advantage of the separability of the problem in parabolic coordinates. Therefore, we seek the solution in the form

$$\Psi_{\tilde{E},M,b}(\xi,\eta,\phi) = F(\xi)G(\eta)\exp(iM\phi). \tag{42}$$

The eigenvalues $\tilde{E}$, M, and b appear as separation constants and can be used to label F and G as well. In the parabolic coordinate system the boundary condition introduced by the mirror simply reads

$$G(\eta) = 0 \quad \text{for} \quad \eta \geq R_M. \tag{43}$$

We now express $\hat{H}$ and $\hat{b}$ in position representation in parabolic coordinates. After a tedious, but straightforward calculation we obtain:

$$\hat{H} = -\frac{\hbar^2}{2m}\left\{\frac{4}{\xi+\eta}\left[\frac{\partial}{\partial\xi}\left(\xi\frac{\partial}{\partial\xi}\right) + \frac{\partial}{\partial\eta}\left(\eta\frac{\partial}{\partial\eta}\right)\right] + \frac{1}{\xi\eta}\frac{\partial^2}{\partial\phi^2}\right\}$$

$$+ \frac{mg}{2}(\xi - \eta), \tag{44}$$

$$\hat{b} = \frac{\hbar^2}{2m}\left\{\frac{4\xi\eta}{\xi+\eta}\left[\frac{1}{\xi}\frac{\partial}{\partial\xi}\left(\xi\frac{\partial}{\partial\xi}\right) - \frac{1}{\eta}\frac{\partial}{\partial\eta}\left(\eta\frac{\partial}{\partial\eta}\right)\right] - \frac{\xi-\eta}{\xi\eta}\frac{\partial^2}{\partial\phi^2}\right\}$$

$$- \frac{mg}{2}\xi\eta. \tag{45}$$

In (44) the zero of the potential energy is taken at the focus of the mirror as in (25). We now consider the two eigenvalue equations (I): $\hat{H}\Psi_{\tilde{E},M,b} = \tilde{E}\Psi_{\tilde{E},M,b}$ and (II): $\hat{b}\Psi_{\tilde{E},M,b} = b\Psi_{\tilde{E},M,b}$. Forming the two quantities (I)+(II)/η

and $(I) - (II)/\xi$, we obtain two independent equations for $F(\xi)$ and $G(\eta)$:

$$\left(\frac{d^2}{d\xi^2} + \frac{1}{\xi}\frac{d}{d\xi} - \frac{M^2}{4\xi^2} - \frac{R_E + \xi}{8z_0^3} - \frac{\beta}{4\xi}\right)F = 0, \quad (46)$$

$$\left(\frac{d^2}{d\eta^2} + \frac{1}{\eta}\frac{d}{d\eta} - \frac{M^2}{4\eta^2} + \frac{\eta - R_E}{8z_0^3} + \frac{\beta}{4\eta}\right)G = 0, \quad (47)$$

where we have used (2) and where we have put

$$R_E = \frac{-2\tilde{E}}{mg} \quad (48)$$

and

$$\beta = 2mb/\hbar^2. \quad (49)$$

Equations (46, 47) are eigenvalue equations for F and G with eigenvalues $R_E/8z_0^3$. The boundary condition (43), associated with $F(+\infty) = 0$, guarantees the existence of non-zero-solutions to (46, 47). The allowed values of β are then determined from the condition that both (46) and (47) must have simultaneous eigenvalues $R_E/8z_0^3$. We note that (46, 47) are similar to the Schrödinger equation for the hydrogen atom in an electric field [20], with the difference that the fractional *charges* $+\beta$ and $-\beta$ are required to add up to 0 instead of 1 as in the Coulomb case.

The simultaneous solution of (46) and (47) requires in general a numerical treatment. In the following, we restrict ourselves to the paraxial regime which seems the most interesting practically. Furthermore, we will be able to get in this case approximate analytical solutions. A complementary regime, where the motion is limited to a region near a ballistic parabola between two points on the mirror, can be treated in a similar fashion.

2.4 The Quantum Motion in the Paraxial Regime

Paraxial motion takes place near the z-axis below the focus of the mirror, i.e., for $\tilde{E} < 0$ corresponding to the classical stability criterion (18). In this region ($\tilde{z} < 0$), we can derive the approximate expressions

$$\xi \simeq \frac{x^2 + y^2}{-2\tilde{z}}, \quad (50)$$

$$\eta \simeq \frac{x^2 + y^2}{-2\tilde{z}} - 2\tilde{z}, \quad (51)$$

for $\xi \ll \eta$. Therefore, η corresponds predominantly to the longitudinal motion, whereas ξ corresponds to the transverse motion, as we have already noticed when studying the classical trajectories.

The paraxial eigenstates can now be defined more precisely by the following requirements:

(*i*) They are located well below the focus of the mirror; more precisely, the distance between the turning point and the focus of the mirror is large compared to z_0, i.e., $R_E \gg z_0$.

(*ii*) They are highly excited with respect to the longitudinal coordinate η; $E = \tilde{E} + mgR_M/2 \gg \hbar\omega_0$, where ω_0 is given in (12).

(*iii*) They correspond to low excitation of the transverse motion, i.e., according to (37) and (49) to small absolute values of β ($\beta < 0$); later on we will see that the precise requirement is $|\beta| \ll R_E/z_0^2$.

a) The Transverse Motion. We consider the transverse motion in the limit of low quantum numbers and for small transverse extension of the wavefunction. For small ξ, we can approximate (46) by neglecting the linear term in $\xi/8z_0^3$. We will check at the end of this calculation that this assumption is consistent with our result. We also change to the new variable

$$\varrho = \sqrt{R_E\xi}$$

so that (46) becomes

$$\left(\frac{d^2}{d\varrho^2} + \frac{1}{\varrho}\frac{d}{d\varrho} - \frac{M^2}{\varrho^2} - \frac{m^2g}{\hbar^2 R_E}\varrho^2 - \frac{\beta}{R_E}\right)F = 0. \quad (52)$$

This is formally identical to the radial Schrödinger equation for a two-dimensional harmonic oscillator with a mass m, an azimuthal quantum number M, a frequency

$$\Omega = \sqrt{\frac{g}{R_E}}, \quad (53)$$

and an energy $\varepsilon = -\hbar^2\beta/2mR_E = -b/R_E$. It is well known that (52) has normalizable solutions only if the following relation holds between ε, M, and Ω:

$$\varepsilon = \hbar\Omega(2n_r + |M| + 1)$$
$$= \hbar\Omega(n_t + 1). \quad (54)$$

The integer $n_r \geq 0$ denotes the number of nodes of the radial function, whereas n_t is the quantum number characterizing the total excitation of the transverse motion. This relation gives us an important connection between the allowed quantized values b and R_E

$$-b = \hbar\sqrt{gR_E}(n_t + 1). \quad (55)$$

We will derive a second relation between b and R_E by studying the longitudinal motion [see (64, 67)] which, combined with (55), determines the allowed values of E and b.

Let us focus here on the *ground state* of (52), corresponding to $M = n_r = n_t = 0$. It is a Gaussian distribution in ϱ:

$$F(\varrho) = \exp(-m\Omega\varrho^2/2\hbar) \quad (56)$$

with a transverse extension given by:

$$\varrho_0^2 = \frac{\hbar}{m\Omega} = \sqrt{2z_0^3 R_E}. \quad (57)$$

The excited states of (52) can be expressed by the well known Laguerre polynomials [13]. We can now check that it is justified to neglect the gravitational term. Had we kept this linear part, we would have obtained a quartic potential in (52) through the replacement

$$\varrho^2 \rightarrow \varrho^2\left(1 + \frac{\varrho^2}{R_E^2}\right). \quad (58)$$

This additional term is thus of the order of ϱ_0^2/R_E^2 $=\sqrt{z_0^3/R_E^3}$ which is indeed small due to assumption (i): $R_E \gg z_0$. This condition also expresses the requirement that the typical transverse energy $\hbar^2/m\varrho_0^2$ is small compared to the energy scale $\hbar^2/mz_0^2$ of the longitudinal motion (see Sect. 1), since $z_0 \ll \varrho_0$ is equivalent to $R_E \gg z_0$ according to (57).

b) The Longitudinal Motion. We now turn to the study of the longitudinal motion in order to determine the allowed quantized values of R_E and thereby the complete set of quantum numbers $\tilde{E}$, b, and M which characterize an eigenstate of the paraxial motion.

In order to solve (47), it is convenient to transform it into a Schrödinger type equation by the change of variables $\eta = e^\mu$ [21, 22]. We then obtain

$$\left[\frac{d^2}{d\mu^2} + e^{2\mu} K^2(\eta = e^\mu) \right] G = 0 \tag{59}$$

with the wave-vector

$$K(\eta) = \left(\frac{\eta - R_E}{8z_0^3} + \frac{\beta}{4\eta} - \frac{M^2}{4\eta^2} \right)^{1/2}. \tag{60}$$

The WKB-solution in the allowed region is given by

$$G(\mu) = \frac{1}{\sqrt{e^\mu K(e^\mu)}} \sin\left(\int_{\mu_{min}}^{\mu} e^{\mu'} K(e^{\mu'}) d\mu' + \frac{\pi}{4} \right). \tag{61}$$

This can be reexpressed in terms of η by

$$G(\eta) = \frac{1}{\sqrt{\eta K(\eta)}} \sin\left[\Phi_{WKB}(\eta) + \frac{\pi}{4} \right], \tag{62}$$

$$\Phi_{WKB}(\eta) = \int_{\eta_{min}}^{\eta} K(\eta') d\eta'. \tag{63}$$

The lower bound $\eta_{min} = \eta_{min}(R_E, \beta, M)$ is the turning point of the η-motion (see Fig. 3c). The WKB quantization condition then reads as

$$\Phi_{WKB}(R_M) = \int_{\eta_{min}}^{R_M} d\eta K(\eta) = \left(n_1 - \frac{1}{4} \right) \pi. \tag{64}$$

Let us now discuss the importance of the three terms contributing to $K(\eta)$ in (60). The first term $(\eta - R_E)/8z_0^3$ is the leading term. If this term was alone, we would recover exactly the same quantization condition as in (7, 9). In this case the wave function would mirror the wave-function (6) yet with parabolic wave fronts $\eta = const$ replacing the plane wave fronts of the plane mirror modes. The second term in (60) describes the correction due to the transverse motion; it is much smaller than the first one, if $\eta - R_E$ is of the order of or larger than z_0 which is the case by virtue of condition (iii). Finally, as long as M^2 is not too large, the last term in $K(\eta)$ is small compared to the two first ones and it will be neglected in the following. We therefore write:

$$K(\eta) \simeq \left(\frac{\eta - R_E}{8z_0^3} \right)^{1/2} + \frac{\beta z_0^{3/2}}{2\eta \sqrt{2(\eta - R_E)}}. \tag{65}$$

Similarly, the position of the turning point η_a is approximately

$$\eta_a \simeq R_E - \frac{2z_0^3 \beta}{R_E}. \tag{66}$$

We can now evaluate the phase integral (63) and then derive the quantization condition. We get after some algebra

$$\Phi_{WKB}(\eta) \simeq \frac{2}{3} \left(\frac{\eta - R_E}{2z_0} \right)^{3/2}$$
$$+ \beta \left(\frac{z_0^3}{2R_E} \right)^{1/2} \arctan\left(\frac{\eta - R_E}{R_E} \right)^{1/2}, \tag{67}$$

where terms small compared to 1 have been neglected. This result plugged into (64) and associated with (55) allows us to determine $\tilde{E}$ and β for a given set of quantum numbers n_1 and n_t for the longitudinal and transverse motions. As an example, we now use these two equations for deriving the frequency spacing between the various modes.

c) Mode Frequency Spacing. In order to calculate the frequency spacing between two adjacent modes (either longitudinal or transverse), we differentiate (55) and (64) to obtain a 2×2 linear system:

$$\Delta n_t = A \Delta R_E + B \Delta \beta, \tag{68}$$

$$\pi \Delta n_1 = C \Delta R_E + D \Delta \beta, \tag{69}$$

where the coefficients A, B, C, D are functions of R_M, R_E, β, and z_0. Keeping only the leading terms in the paraxial approximation, we get

$$A = -\frac{\beta}{2R_E\beta_0}, \quad B = \frac{1}{\beta_0}, \quad C = -\frac{\sqrt{R_M - R_E}}{(2z_0)^{3/2}},$$
$$D = -\frac{1}{\beta_0} \arctan\left(\frac{R_M - R_E}{R_E} \right)^{1/2} \tag{70}$$

with $\beta_0 = -\sqrt{2R_E/z_0^3}$. Let us first consider the spacing between two longitudinal modes. In (68, 69) we set $\Delta n_1 = 1$, $\Delta n_t = 0$. We get $\Delta R_E = \pi(C - DA/B)^{-1} \simeq \pi/C$, and we now use $R_E = -2\tilde{E}/mg$ to obtain

$$\Delta\tilde{E}_1 \simeq 2\pi\hbar \left[\frac{g}{4(R_M - R_E)} \right]^{1/2} \tag{71}$$

which is equivalent to the result (13).

We now set $\Delta n_1 = 0$, $\Delta n_t = 1$ to determine the frequency spacing between transverse modes. We obtain $\Delta R_E = (A - BC/D)^{-1} \simeq -D/BC$ so that

$$\Delta\tilde{E}_t \simeq \left[\frac{1}{\pi} \arctan\left(\frac{R_M - R_E}{R_E} \right)^{1/2} \right] \Delta\tilde{E}_1. \tag{72}$$

This means that the splitting between transverse modes $\Delta\tilde{E}_t$ may be of the same order as the splitting between longitudinal modes $\Delta\tilde{E}_1$, $\Delta\tilde{E}_t = \frac{1}{4}\Delta\tilde{E}_1$ for $R_E = R_M/2$.

+ F   + F

a   b
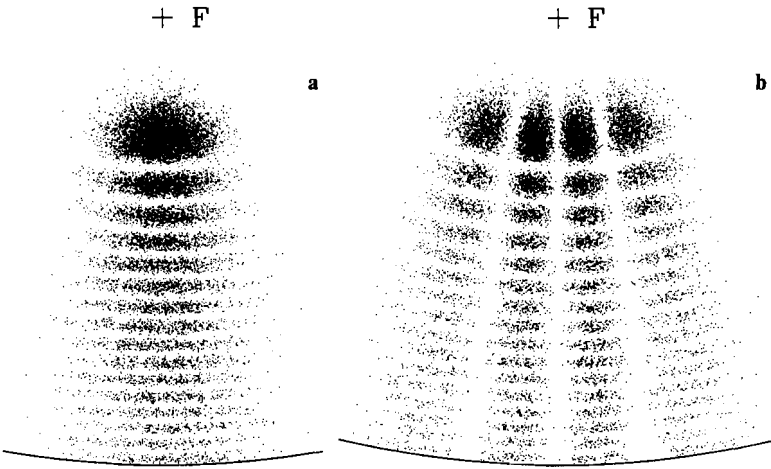
Fig. 4a, b. Density profile for the eigenmode corresponding to the 16th excited state of the longitudinal motion ($R_M/2 = 23z_0$, $z_E = 17.67z_0$). a Ground state of the transverse motion; b excited state $n_r = 1$, $M = 1$ of the transverse motion. F is the focus of the mirror

2.5 Paraxial States in Cartesian Coordinates

We now write the expressions obtained for the paraxial states (56) and (62) in terms of cartesian coordinates. This will allow us in the next Sect. 2.6 to compare our results with the well known characteristics of an optical cavity.

We start with the longitudinal motion. Using (51), the WKB phase (67) is approximately

$$\Phi_{WKB}(x, y, z) \simeq \frac{2}{3}\left(\frac{z_E - z}{z_0}\right)^{3/2}$$
$$\times \left[1 + \frac{3}{4}\frac{x^2 + y^2}{(R_M - 2z)(z_E - z)}\right] + \phi(z), \quad (73)$$

where

$$\phi(z) = \beta \left[\frac{z_0^3}{2(R_M - 2z_E)}\right]^{1/2} \arctan\left[\frac{2(z_E - z)}{R_M - 2z_E}\right]^{1/2}. \quad (74)$$

We have put $z_E = E/mg = (R_M - R_E)/2$. As in Sect. 1, z_E represents the maximal height reached classically by the atom moving with an energy E in the paraxial limit. We now introduce, as in Sect. 1, the local wave vector $k(z)$ $= \sqrt{(z_E - z)/z_0^3}$ so that the function $G(z)$ reads

$$G(x, y, z) = \frac{1}{\sqrt{k(z)}} \frac{1}{\sqrt{R_M - 2z}}$$
$$\times \sin\left[\int_z^{z_E} dz'k(z') + k(z)\frac{x^2 + y^2}{2R(z)} + \phi(z) + \frac{\pi}{4}\right] \quad (75)$$

with

$$R(z) = R_M - 2z. \quad (76)$$

We have thus separated a vertical (longitudinal) phase variation involving both the varying de Broglie wavelength and the additional phase $\phi(z)$, and a transverse phase variation corresponding to a spherical wave with a radius of curvature $R(z)$. This radius of curvature matches the radius of the mirror R_M at $z = 0$ and decreases with increasing z to take its minimal value $R_M - 2z_E$ at the turning point.

The transverse amplitude of the wave function is, on the other hand, determined by the function $F(\xi)$. Using

$\varrho = \sqrt{\xi R_E}$ and the approximation (50) we can rewrite the *ground state* Gaussian wave function $\exp(-\varrho^2/2\varrho_0^2)$ as

$$F(x, y, z) = \exp\left[-\frac{x^2 + y^2}{2w^2(z)}\right], \quad (77)$$

where the transverse area of the wave function varies as

$$w^2(z) = (R_M - 2z)\left(\frac{2z_0^3}{R_M - 2z_E}\right)^{1/2}. \quad (78)$$

The *waist* of the mode at the turning point takes the value

$$w_E = w(z_E) = [2z_0^3(R_M - 2z_E)]^{1/4}. \quad (79)$$

The maximum transverse extension is reached at the mirror ($z = 0$) and is equal to

$$w(z = 0) = z_0\left[\frac{2R_M^2}{z_0(R_M - 2z_E)}\right]^{1/4}. \quad (80)$$

This is the diffraction limited minimum spotsize of a de Broglie wave retroreflected into itself by a parabolic mirror on one side and by gravity on the other side. We remark that this transverse size of the wave function ranges between the *quantum scale* z_0 and the macroscopic scales R_M and R_E. For a typical situation well inside the stability region $z_E = \overline{OF}/2 = R_M/4$, we find from (79, 80) that the waist on the mirror is $\sqrt{2}$ larger than the waist around the turning point. Numerical values for this waist in the case $R_M = 2$ cm, $z_E = 5$ mm and for the three atoms He*, Na, Cs are indicated in Table 1.

Figures 4a and 4b give examples of atomic density plots for two paraxial modes calculated using the results of this section.

2.6 Gaussian Beam Analogy

The paraxial solution obtained above for the Schrödinger equations (46, 47) describes essentially an atomic de Broglie wave propagating vertically up and down with a small transverse diffraction. It is instructive to compare such a de Broglie wave with the solution obtained from a Gaussian beam approach, similar to the one used

in optics [12, 14], the gravitational potential playing here the role of a z-dependent index of refraction.

Formally, the solution of the three-dimensional Schrödinger equation

$$[\Delta + k^2(z)]\Psi(x, y, z) = 0 \qquad (81)$$

with $k^2(z) = (z - z_E)/z_0^3$ is sought in analogy to the description of optical wave propagation by the ansatz

$$\Psi(x, y, z) = \Psi_{0\pm}(z)\Psi_1(x, y, z), \qquad (82)$$

where

$$\Psi_{0\pm}(z) = \frac{1}{\sqrt{k(z)}}\exp\left[\pm i\left(\int_z^{z_E} dz' k(z') + \frac{\pi}{4}\right)\right] \qquad (83)$$

contains the rapid phase variation in the direction of propagation (cf. Sect. 1) and where Ψ_1 contains the slowly varying amplitude and phase factors which determine the beam shape and the curvature of the wavefronts. Neglecting slowly varying terms, (81) leads to the approximate equation for Ψ_1:

$$\left(\frac{\partial^2}{\partial x^2} + \frac{\partial^2}{\partial y^2} - 2ik(z)\frac{\partial}{\partial z}\right)\Psi_1(x, y, z) = 0. \qquad (84)$$

This can be reduced to the standard form with a constant wave vector

$$\left(\frac{\partial^2}{\partial x^2} + \frac{\partial^2}{\partial y^2} + ik_E\frac{\partial}{\partial \theta}\right)\Psi_1(x, y, \theta) = 0 \qquad (85)$$

if we introduce the new longitudinal variable $\theta(z) = \sqrt{z_E(z_E - z)}$ which is proportional to the time of free fall from z_E to z. In (85), $k_E = \sqrt{z_E/z_0^3}$ is the maximum wave vector of the atom reached at the position of the mirror.

The general solution of (85) is well known. It corresponds to a Gaussian beam characterized by its focal plane and its waist. To determine such a solution one needs two boundary conditions. For the present problem, one of these conditions is obtained by requiring the radius of curvature of the beam to match the radius of curvature R_M of the mirror in $z = 0$ ($\theta = z_E$). It does not seem easy to find convincing arguments for specifying the second boundary condition, for example, the radius of curvature of the wave at the turning point $z = z_E$ ($\theta = 0$).

We have thus found it necessary to start from the solution obtained in the parabolic coordinate treatment (75) and (77), to rewrite it in terms of x, y, and θ and to check that it matches the usual Gaussian beam solutions of (85).

Restricting ourselves to the ground state for the ξ-motion, we obtain for the function $\Psi_{\tilde{E},0,b}$ deduced from (75, 77): $\Psi_{\tilde{E},0,b} = \Psi_{0\pm}(z)\Psi_1(x, y, \theta) + \text{c.c.}$ with

$$\Psi_1(x, y, \theta) = \frac{1}{w(\theta)}\exp\left(-\frac{x^2 + y^2}{2w^2(\theta)}\right)$$
$$\times \exp\left[-i\left(\frac{k_E(x^2 + y^2)}{2\bar{R}(\theta)} + \arctan\frac{\theta}{\theta_R}\right)\right]. \qquad (86)$$

This indeed corresponds to the TEM$_{00}$ Gaussian beam solution of (85) with a focal plane located at $\theta = 0$, i.e., at

the turning point $z = z_E$, with a beam *diameter* of

$$w(\theta) = w_E\left[1 + \left(\frac{2\theta}{k_E w_{E^2}}\right)^2\right]^{1/2}, \qquad (87)$$

with a Rayleigh length $\theta_R = k_E w_E^2/2$, and with a radius of curvature of

$$\bar{R}(\theta) = \frac{2(\theta^2 + \theta_R^2)}{\theta}. \qquad (88)$$

Using the result (79) for w_E, one can check that the radius of curvature on the mirror $\bar{R}(\theta = z_E)$ matches the radius of curvature of the mirror R_M.

Let us finally point out a conceptual difference between the radius of curvature $R(z)$ defined in (76) and the one introduced here, $\bar{R}(\theta)$. The first one corresponds to the local wave vector $k(z)$ as it appears in (75). It gives the shape of the wavefronts in real space (x, y, z); in particular it is finite around the turning point, the corresponding nodal surface being a parabola $\eta = R_E$. The radius of curvature $\bar{R}(\theta)$, defined in the fictitious space (x, y, θ) refers to a constant wave vector k_E which coincides with the real one $k(z)$ only on the surface of the mirror. This radius of curvature $\bar{R}(\theta)$, which is infinite around the turning point, has therefore no direct geometrical significance.

3 Injecting Atoms in the Cavity Modes

We now come to the last part of this paper, which deals with the calculation of the number of modes which will be populated if one starts from an atomic cloud, produced for instance by a molasses or a magnetooptic trap. This problem is of particular interest if one wants to accumulate several atoms in a few modes, in order to achieve high degeneracy factors and therefore to be in a situation where collective effects due to quantum statistics may play a role.

We will assume here that the initial atomic phase space distribution (Wigner distribution) is Gaussian both in the spatial and momentum variables x, y, z and p_x, p_y, p_z. This distribution is supposed to be centered on the z-axis at a height z_E above the surface of the mirror. We then have

$$W(\mathbf{r}, \mathbf{p}) = W_x(x, p_x)W_y(y, p_y)W_z(z, p_z) \qquad (89)$$

with, for instance,

$$W_z(z, p_z) = \frac{1}{2\pi z_i p_{zi}}\exp[-(z - z_E)^2/2z_i^2]$$
$$\times \exp(-p_z^2/2p_{zi}^2). \qquad (90)$$

The position and momentum widths satisfy the Heisenberg inequalities $x_i p_{xi}, y_i p_{yi}, z_i p_{zi} \geq \hbar/2$. The situation $x_i p_{xi} = \ldots = \hbar/2$ is of particular interest, since it corresponds to a pure state $|\psi_{in}\rangle$ (Gaussian wave packet). However, it should be kept in mind that most of the atomic clouds produced in present experiments are far from this limit. For instance, a magnetooptic trap for Cesium atoms [23, 24] leads, at best, to a radius $r_i \simeq 50$ μm with a rms momentum p_i of $p_i/m \simeq 2$ cm/s; this leads to $r_i p_i \simeq 2000\hbar$, far from a pure state! We also assume here

that all the relevant points of these phase space distributions are well inside the stability region, that is, $z_E < R_M/2$ and $z_i \ll R_M/2 - z_E$.

We first calculate the overlap of this initial distribution with the Gaussian ground state of the transverse motion. We then evaluate the number of longitudinal modes that are populated, and we finally briefly discuss the conditions under which high degeneracy factors can be achieved.

3.1 The Population of the Transverse Ground State Mode

We suppose here that the initial distribution is symmetric with respect to x and y and we put $r_i = x_i = y_i$ and $p_i = p_{xi} = p_{yi}$. If we denote ϱ_t the initial atomic density matrix corresponding to the transverse x-y degrees of freedom, the population π_0 of the transverse ground state mode $F(x, y, z)$ (77) is given by

$$\pi_0 \simeq \frac{1}{\pi w_E^2} \int dx\, dx'\, dy\, dy'$$

$$\times F^*(x, y, z_E) F(x', y', z_E) \langle x, y | \varrho_t | x', y' \rangle. \tag{91}$$

We have used here the fact that the z extension of the initial distributions is small so that the variation with z of the waist $w(z)$ of F can be neglected. Strictly speaking, we should also incorporate in (91) the transverse phase variation of the cavity modes appearing in the expression (75) of G. However, the radii of curvature involved are much larger than the waist w_E and the contribution of these terms is therefore negligible.

The density matrix element $\langle x, y | \varrho_t | x', y' \rangle$ is simply obtained by a Fourier transform of (89, 90)

$$\langle x, y | \varrho_t | x', y' \rangle = \sigma(x, x') \sigma(y, y') \tag{92}$$

with

$$\sigma(x, x') = \int dp_x\, e^{ip_x(x-x')/\hbar} W\left(\frac{x+x'}{2}, p_x\right)$$

$$= \frac{1}{r_i \sqrt{2\pi}} \exp\left[-\frac{(x+x')^2}{8r_i^2}\right] \exp\left[-\frac{p_i^2(x-x')^2}{2\hbar^2}\right]. \tag{93}$$

In the case of an initial distribution corresponding to a pure state $\psi_{in}(x)$ $(r_i p_i = \hbar/2)$ this factorizes in the product of two functions depending on x and x': $\sigma(x, x') = \psi_{in}(x) \psi_{in}^*(x')$, respectively.

The integral (91) only involves Gaussian functions and can be calculated simply. In the limiting case $r_i p_i = \hbar/2$, we obtain

$$\pi_0 = 8 \left(\frac{r_i w_E}{2r_i^2 + w_E^2}\right)^2 \tag{94}$$

which can be equal to 1 if the initial Gaussian distribution perfectly matches the Gaussian transverse mode $(r_i = w_E/\sqrt{2})$. In the general case, we obtain

$$\pi_0 = \frac{\hbar^2}{(r_i^2 + w_E^2/2)(p_i^2 + \hbar^2/2w_E^2)}. \tag{95}$$

This is always much smaller than 1 if $r_i p_i \gg \hbar$. For the cesium magnetooptic trap considered above and for a typical cavity as the one described at the end of Sect. 2, we find $\pi_0 \simeq 2.5 \times 10^{-7}$. This very small number could be increased by a further reduction of the momentum dispersion p_i and by a better confinement of the atom using, for instance, a dipole laser trap consisting of a tightly focused laser beam with a beam waist smaller than w_E. Those two features could be combined by using, just before releasing the atoms, an adiabatic opening of this confining trap so that the value of r_i would increase up to w_E, while, at the same time, p_i would decrease due to the conservation of $r_i p_i$ in the adiabatic opening.

3.2 The Population of the Longitudinal Modes

The population of a given longitudinal mode could be calculated in the same way as we have done for the transverse case, by evaluating an integral similar to (91). However, our purpose here is more to estimate the number Δn_l of longitudinal modes that are excited rather than determining the population of a given one. In order to calculate Δn_l we proceed in two steps. First, we estimate the energy spread ΔE of our initial distribution and second, we use

$$\Delta n_l = \frac{\Delta E}{(\partial E/\partial n)_{E = \bar{E}}}, \tag{96}$$

where $(\partial E/\partial n)_{E = \bar{E}}$ is the density of modes around the average initial energy $\bar{E}$ [see (13)]. The energy spread ΔE is defined by

$$(\Delta E)^2 = \langle H_z^2 \rangle - \langle H_z \rangle^2 \tag{97}$$

with $H_z = p_z^2/2m + mgz$. This quantity is easily calculated from the Wigner representation of the initial distribution (89, 90)

$$\Delta E = \left(\frac{p_{zi}^4}{2m^2} + m^2 g^2 z_i^2\right)^{1/2}$$

$$= mgz_0 \sqrt{2\left(\frac{z_0}{\lambda_{dB}}\right)^4 + \left(\frac{z_i}{z_0}\right)^2}, \tag{98}$$

where we have introduced the reduced de Broglie wavelength $\lambda_{dB} = \hbar/p_{z_i}$. Combining (98) with (13) gives the value of Δn_l

$$\Delta n_l = \frac{1}{\pi} \sqrt{\frac{z_E}{z_0}} \sqrt{2\left(\frac{z_0}{\lambda_{dB}}\right)^4 + \left(\frac{z_i}{z_0}\right)^2}. \tag{99}$$

Let us discuss the two limiting cases $z_i p_{zi} = \hbar/2$ (pure state) and $r_i p_i \gg \hbar/2$. For a pure case we find that ΔE is minimum when $z_i = 2^{-1/3} z_0$. In this case we get

$$\Delta n_l = 2^{-5/3} \left(\frac{3z_E}{\pi^2 z_0}\right)^{1/2} \simeq 0.29 \bar{n}^{1/3}, \tag{100}$$

where $\bar{n}$ is the average longitudinal quantum number. We recall that a typical $\bar{n}$ is 10^5–10^6 (see Table 1) which gives for this optimal initial pure state about 30 excited modes.

This result has been confirmed by a direct calculation of the integral of overlap of the initial state with the Airy-functions (4). In the case where $z_i p_{z_i} \gg \hbar/2$, e.g., if we again consider the cesium magnetooptic trap described above, the two terms of (98) are of the same order and lead to $\Delta n_1 \simeq 10^4$.

3.3 Comparison with the Two-Mirror Cavity

We now briefly compare the previous results with those obtained for a linear two-mirror cavity [7] in which we neglect gravity. The calculation for the transverse modes is the same as for an optical cavity and leads to typical waists of the order of a few microns, for a cavity length $L \simeq 1$ cm and a longitudinal velocity $v \simeq 1$ m/s. The calculation of the population π_0 of the ground transverse mode remains valid and leads to equations identical to (94) and (95).

The number Δn_1 of populated longitudinal modes is still given by (96) but we must now use the relation $E = n_1^2 \pi^2 \hbar^2 / 2mL^2$ between the energy E and the longitudinal quantum number n_1. If we denote Δp the initial atomic momentum dispersion around the average momentum $\bar{p}$ $(\bar{p} = n_1 \pi \hbar / L)$, we find

$$\Delta n_1 \simeq \frac{L}{\pi \hbar} \Delta p. \tag{101}$$

If the atoms are injected in the cavity using moving molasses, Δp is as above, of the order of a few recoil momenta. This gives, typically, $\Delta n_1 \simeq 10^5$, larger by one order of magnitude than the one found for a gravitational gravity.

3.4 Achievement of High Degeneracy Factors

Quantum statistical effects are expected to be important when the number N_v of atoms in a given mode v is larger than 1. This degeneracy factor N_v plays a role analogous to the one defined for Bose-Einstein condensation $n \lambda_{dB}^3$, where n is the density of an ensemble of free atoms at temperature T and λ_{dB} is their de Broglie wavelength. In both cases the goal is to achieve degeneracy factors as high as possible ($\gg 1$), while, at the same time, keeping the density low enough to avoid losses due to collision effects. In this section we show that it is possible to achieve, in a gravitational cavity, degeneracy factors higher than in the optical molasses used for filling the cavity if one combines repeated fillings with suitable mode selection.

Consider an atomic cloud of N atoms with a phase space density (90) in the isotropic case. The degeneracy factor is

$$n \lambda_{dB}^3 \simeq \frac{N \hbar^3}{r_i^3 p_i^3}. \tag{102}$$

If this cloud is dropped in a gravitational cavity, the maximal population of a mode corresponding to the ground state of the transverse motion is, using (95) and

(99), in the case $r_i > w_E$, $p_i > \hbar/w_E$

$$N_v = \frac{N \pi_0}{\Delta n_1}$$

$$= N \frac{\pi \hbar^2}{p_i^2 r_i^2} \left[2 \left(\frac{z_0}{\lambda_{dB}} \right)^4 + \left(\frac{r_i}{z_0} \right)^2 \right]^{-1/2} \sqrt{\frac{z_0}{z_E}}. \tag{103}$$

As expected, N_v increases when λ_{dB} increases (colder atoms) and when r_i decreases (smaller clouds). The lowest achievable 3D temperature achieved in laser cooling leads to a λ_{dB} of a fraction of an optical wavelength. The smallest present values of r_i are of the order of a typical laser beam waist (10–50 µm). The values of λ_{dB} and r_i being roughly the same for all laser cooled atoms, we now look for the value of z_0, i.e., of the atomic mass, optimizing N_v. We find $z_0^{opt} \simeq (\lambda_{dB}^2 r_i/2)^{1/3} \simeq 0.5$ µm which is in the range of the values found for Na and Cs (see Table 1). Using these values of z_0^{opt}, one gets

$$N_v^{opt} \simeq \frac{N \hbar^3}{r_i^3 p_i^3} \sqrt{\frac{r_i}{3 z_E}} \tag{104}$$

which is smaller than (102) by a factor of $\sqrt{r_i/z_E}$.

To increase N_v^{opt}, one can consider multiple fillings of the cavity (using for example hyperfine optical pumping for inserting new atoms in the cavity modes without blowing out atoms which are already present). Suppose, for example, that we repeat $\sqrt{z_E/r_i}$ fillings so that we recover the initial degeneracy factor (102). We evaluate now the maximal spatial density in the cavity. Consider first a single filling. After a while, the atoms initially in an altitude range z_i are distributed between $z = 0$ and $z = z_E$. From the WKB wave function, one knows that the maximum density is found around the turning point and is reduced by a factor of $\sqrt{r_i/z_E}$ with respect to the initial density. Consequently, after $\sqrt{z_E/r_i}$ fillings we also recover the initial density of the atomic cloud. To sum up these arguments, in such a *free running* cavity we cannot increase the degeneracy factor without increasing, at the same time, the density of the atomic cloud.

An attractive solution for circumventing such a difficulty is to insert some *mode selective* elements into the cavity which would remove the atoms from most modes, except a few, reducing then the density without changing N_v^{opt}. One could then increase considerably the number of fillings, and therefore the degeneracy factor, without being limited again by collisional losses.

4 Conclusion

In this paper we have presented the quantum mechanical description of a parabolic gravitational cavity. The eigenmodes of such a cavity, corresponding to three-dimensional standing de Broglie waves for the center of mass, have been determined. In the limit of paraxial motion, which is stable if the apex of the classical trajectory is below the focus of the mirror, we have found simple eigenfunctions: they consist of Airy-functions along the vertical axis and of 2D harmonic oscillator

eigenfunctions in the transverse directions. The treatment presented in this paper can be extended outside the paraxial domain, using the separability of the problem in parabolic coordinates.

Populating a small number of modes from a source of cold atoms and achieving high degeneracy factors is an important problem which has also been addressed. The conclusion of our analysis is that mode selection mechanisms are required if one wants to achieve high degeneracy factors with densities low enough to avoid collisional losses. Such a mode selection could, for example, operate exploiting velocity selective Raman transitions between two atomic internal states [25]. Note finally, that a direct observation of the mode structure analyzed here would represent the first observation of a multiple wave atomic interferometer.

References

1. For a recent overview see, e.g.: *Laser Cooling and Trapping of Atoms,* ed. by S. Chu, C. Wieman (Special Issue, J. Opt. Soc. Am. B6, 1989)
2. M.A. Kasevich, E. Riis, S. Chu, R. DeVoe: Phys. Rev. Lett. **63**, 612 (1990)
3. A. Clairon, C. Salomon, S. Guellati, W. Phillips: Europhys. Lett. **16**, 165 (1991)
4. Th. Walker, D. Sesko, C. Wieman: Phys. Rev. Lett. **64**, 408 (1990)
5. T.J. Greytak, D. Kleppner: In *New Trends in Atomic Physics,* ed. by G. Grynberg, R. Stora (North-Holland, Amsterdam 1984) p. 1125
6. J.T.M. Walraven: In *Fundamental Systems in Quantum Optics* (1990), ed. by J. Dalibard, J.M. Raimond, J. Zinn-Justin (North-Holland, Amsterdam, to appear in 1992)
7. V.I. Balykin, V.S. Letokhov: Appl. Phys. B **48**, 517 (1989)
8. R. Cook, R. Hill: Opt. Commun. **43**, 258 (1982)
9. V.I. Balykin, V.S. Letokhov, Yu.B. Ovchinnikov, A.I. Sidorov: Phys. Rev. Lett. **60**, 2137 (1988)
10. J.J. Berkhout, O.J. Luiten, I.D. Setija, T.W. Hijmans, T. Mizusaki, J.T.M. Walraven: Phys. Rev. Lett. **63**, 1689 (1989)
11. M.A. Kasevich, D.S. Weiss, S. Chu: Opt. Letters **15**, 607 (1990). In this reference the authors also mention an unpublished theoretical analysis of a gravitational cavity
12. For a general propagator approach to the motion of nonrelativistic particles in gravitational or inertial fields, see: C. Bordé: In *Fundamental Systems in Quantum Optics,* ed. by J. Dalibard, J.M. Raimond, J. Zinn-Justin (North-Holland, Amsterdam, to appear in 1992)
13. M.A. Abramowitz, I.A. Stegun: *Handbook of Mathematical Functions* (Dover, New York 1972)
14. H. Kogelnik, T. Li: Appl. Opt. **5**, 1550 (1966)
15. L.D. Landau, E.M. Lifshitz: *Mechanics* (Pergamon, Oxford 1976)
16. H.J. Korsch, J. Lang: J. Phys. A **24**, 45 (1991)
17. P. Lett, W. Phillips, S. Rolston, C. Tanner, R. Watts, C. Westbrook: J. Opt. Soc. Am. B**6**, 2084 (1989)
18. D.S. Weiss, E. Riis, Y. Shevy, P.J. Ungar, S. Chu: J. Opt. Soc. Am. B**6**, 2072 (1989)
19. C. Salomon, J. Dalibard, W. Phillips, A. Clairon, S. Guellati: Europhys. Lett. **12**, 683 (1990)
20. E. Schrödinger: Ann. d. Phys. **80**, 437 (1926)
21. R.E. Langer: Phys. Rev. **51**, 669 (1937)
22. M.V. Berry, K.E. Mount: Rep. Prog. Phys. **35**, 315 (1972)
23. C. Foot, A. Steane: Europhys. Lett. **14**, 231 (1990)
24. C. Salomon: E.N.S. (private communication)
25. M.A. Kasevich, D.S. Weiss, E. Riis, K. Moler, S. Kasapi, S. Chu: Phys. Rev. Lett. **66**, 2297 (1991)